Atmos. Chem. Phys. Discuss., 13, 22893–22930, 2013
www.atmos-chem-phys-discuss.net/13/22893/2013/
doi:10.5194/acpd-13-22893-2013


Atmospheric Chemistry and Physics Discussions



# Temporal changes in the emissions of $CH_4$ and CO from China estimated from $CH_4/CO_2$ and $CO/CO_2$ correlations observed at Hateruma Island

**Y. Tohjima[1], M. Kubo[2], C. Minejima[3], H. Mukai[1], H. Tanimoto[1], A. Ganshin[4], S. Maksyutov[1], K. Katsumata[1], T. Machida[1], and K. Kita[2]**

[1]Center for Global Environmental Research, National Institute for Environmental Studies, Tsukuba, Japan
[2]Faculty of Science, Ibaraki University, Mito, Japan
[3]Department of Chemical Engineering, Tokyo University of Agriculture and Technology, Tokyo, Japan
[4]Central Aerological Observatory, Dolgoprudny, Russia

Received: 22 August 2013 – Accepted: 22 August 2013 – Published: 30 August 2013

Correspondence to: Y. Tohjima (tohjima@nies.go.jp)

Published by Copernicus Publications on behalf of the European Geosciences Union.







## Abstract

In-situ observation of the atmospheric $CO_2$, $CH_4$, and CO mixing ratios at Hateruma Island (HAT, 24.05° N, 123.80° E) often show synoptic-scale variations with correlative elevations during winter, associated with air transport from the East Asian countries. We examine winter (November-March) trends in $\Delta CH_4 / \Delta CO_2$, $\Delta CO / \Delta CO_2$, and $\Delta CO / \Delta CH_4$ observed at Hateruma over the period 1999 to 2010. Although the ratios $\Delta CH_4 / \Delta CO_2$ and $\Delta CO / \Delta CO_2$ both show an overall gradual decrease over the study period due to a recent rapid increase in fossil fuel consumption in China, we note that $\Delta CH_4 / \Delta CO_2$ and $\Delta CO / \Delta CO_2$ remains relatively flat (no trend) during 2005–2010 and 1999–2004, respectively. The $CO/CH_4$ slope on the other hand shows an increasing trend during 1999–2004 but a decrease during 2005–2010. Calculation of the concentration footprint for the atmospheric observation at HAT by using the FLEXPART Lagrangian particle dispersion model indicates that most of the short-term variations are caused by emission variations from North and East China. Combined with a set of reported emission maps, we have estimated the temporal changes in the annual $CH_4$ and CO emissions from China under the assumption that the estimate of the fossil fuel-derived $CO_2$ emissions based on the energy statistics is accurate. The estimated annual $CH_4$ emissions, corresponding to non-seasonal sources or anthropogenic sources without rice fields, show a nearly constant value of $39 \pm 6$ $TgCH_4\,yr^{-1}$ during 1998–2002, and then gradually increases to $46 \pm 7$ $TgCH_4\,yr^{-1}$ in 2009/2010. The estimated annual CO emissions increase from $134 \pm 26$ $TgCO\,yr^{-1}$ in 1998/1999 to $182 \pm 33$ $TgCO\,yr^{-1}$ in 2004/2005, level off after 2005, and then slightly decrease to less than 160 $TgCO\,yr^{-1}$ in 2008–2010.

## 1 Introduction

Methane ($CH_4$) is the second most important greenhouse gas in the atmosphere after carbon dioxide ($CO_2$). Analyses of ancient air occluded in polar ice core samples have





ACPD
13, 22893–22930, 2013



suggested that atmospheric $CH_4$ has more than doubled since the preindustrial period (e.g., Etheridge, et al., 1998; Nakazawa et al., 1993). This long-term increase can be attributed to increases in anthropogenic sources (e.g., fossil fuels, domestic ruminants, and rice fields). Resent systematic measurements of atmospheric $CH_4$ have shown a slowing down in the rate of increase after 1980s with a significant interannual variability (Steele et al., 1992; Dlugokencky et al., 1998), leveling off in the early 2000s (Dlugokencky et al., 2003), and an abrupt renewed increase after 2007 (Rigby et al., 2008; Dlugokencky et al., 2009; Terao et al., 2011). These temporal changes in atmospheric $CH_4$ is a result of an overall balance between the emission and the destruction by hydroxyl radical (OH) in the atmosphere.

Carbon monoxide (CO), produced during incomplete combustion of fossil fuels and biomass, is an atmospheric pollutant. CO also plays an important role in atmospheric chemistry. The CO reaction with OH, a dominant sink for atmospheric CO, removes about 75 % of OH in the atmosphere (Thompson, 1992), influencing the atmospheric oxidation capacity. Therefore, changes in the CO emission could indirectly affect the atmospheric levels of $CH_4$ and other greenhouse gases that are removed by OH (e.g., Logan et al., 1981). Depending on the levels of the mixing ratios of nitrogen oxides ($NO_x$), CO could act as a source for tropospheric ozone, which is also a greenhouse gas. Since both $CH_4$ and CO have the potential to affect directly and indirectly the global climate, it is crucial to understand their changing emissions with time by obtaining better spatio-temporal information about their surface fluxes.

In terms of regional emissions of greenhouse gases and pollutants, East Asia is one of the most important regions in the world because of the positive association between anthropogenic emissions and the recent rapid economic growth in the region. For example, fossil fuel-derived $CO_2$ emissions in China have more than doubled over the recent decade (Fig. 1), and passed the United States as the world's largest fossil $CO_2$ emitter in 2006 (Gregg et al., 2008). The increases in the fossil $CO_2$ emissions from China will also likely lead to enhanced emissions of other chemical species related to fossil fuel combustion. The recently revised EDGAR Ver. 4.2 (Emission Database





ACPD
13, 22893–22930, 2013



for Global Atmospheric Research, http://edgar.jrc.ec.europa.eu/) inventory database shows an increase in the estimated anthropogenic $CH_4$ and CO emissions from China after 2003 (Fig. 1b and c). These increases are mostly related to $CH_4$ from fossil fuels and CO from the sectors of manufacturing industry and metal production. However, the $CH_4$ and CO emission inventories are considered to be more uncertain than the fossil $CO_2$ emission inventory because of the uncertainty and variability of the emission factors and the heterogeneity of the emission distributions. These emission increases will result in a corresponding elevation in the mixing ratios of $CH_4$, CO, and $CO_2$ in the downwind region of the sources.

In the downwind from source regions, it has been observed that various chemical species with similar or same sources are highly correlated on a synoptic time scale. That is, a synoptic-scale variation (SSV) in the mixing ratio of one chemical species is usually associated with SSVs of other species that have similar regional emission distributions and atmospheric lifetime characteristics. Therefore, various combinations of specific chemical species with relatively well known quantified sources or relationships can be used to constrain emission estimates of other species with poorly quantified source strengths. For example, atmospheric Radon-222 measurements have been used to constrain regional fluxes of such greenhouse gases as $CO_2$ and $CH_4$ (e.g. Levin et al., 2003; Schmidt et al., 2003; Wada et al., 2013). Worthy et al. (2009) estimated the interannual variation in anthropogenic $CH_4$ emissions from Europe and Siberia based on the $CH_4/CO_2$ correlations observed at Alert. Yokouchi et al. (2006) estimated the emission strength of hydrofluorocarbons and halocarbons from East Asian countries based on their correlations with atmospheric CO observed at Hateruma Island.

The National Institute for Environmental Studies (NIES) has been carrying out in-situ measurements of atmospheric greenhouse gases and pollutants, including $CO_2$, $CH_4$, and CO at Hateruma Island (HAT; 24.05° N, 123.80° E), which is located off the coast of the East Asian continent. During the period from late fall to early spring, HAT is mainly influenced by the air masses transported from East Asian countries, resulting in





ACPD
13, 22893–22930, 2013



highly associated SSV events of enhanced mixing ratios of atmospheric $CO_2$, $CH_4$ and CO. Using the observed $CO_2$ and $CH_4$ SSVs at HAT during winter (November–April), Tohjima et al. (2010) found that the ratio of the standard deviations of deseasonalized $CO_2$ and $CH_4$ ($\sigma_{CO_2}/\sigma_{CH_4}$) gradually increased during 1996–2007, reflecting changes in the fossil $CO_2$ emissions from China.

In this study, in addition to revisiting the analysis of $CO_2$ and $CH_4$ at HAT, we have extended our study to include an analysis of the correlation between CO and $CO_2$ by using hourly data instead of daily averages, as was done in a previous study by Tohjima et al. (2010). By calculating the temporal variations in the ratios of $\Delta CH_4 / \Delta CO_2$, $\Delta CO / \Delta CO_2$, and $\Delta CO / \Delta CH_4$ from the observed measurements at HAT over the period from 1997/1998 to 2010, and combining them with the footprint results for different gases from a Lagrangian particle dispersion model (FLEXPART) and the existing flux maps of $CH_4$, CO and $CO_2$, we are able to improve the estimate of the spatio-temporal distributions of these trace gases and their source strengths in the continental Asia.

## 2 In-situ observation at Hateruma Island

We have been monitoring atmospheric $CO_2$, $CH_4$ and CO at HAT by using automated analytical systems, which have been described elsewhere by Mukai et al. (2001) for $CO_2$, by Tohjima et al. (2002) for $CH_4$, and Tanimoto et al. (2009) for CO. Therefore, we give only an outline description of these analytical systems.

Two air intakes (inverted cylindrical beakers), one for $CO_2$ and the other for $CH_4$ and CO measurements, are placed at the top of a tower at a height of 36.5 m (46.5 m above sea level), and sample air is drawn in through a 3/8-inch stainless steel tubing by diaphragm pumps placed inside the station building.

The sample air for $CO_2$ measurement is dried by passing it through 3 cold traps (2 °C, −40 °C and −70 °C). $CO_2$ is continuously measured by a nondispersive infrared analyzer (NDIR) (URA207, Shimadzu CO. Ltd., Japan) with an analytical precision of about 0.02 µmol mol$^{-1}$ (ppm). $CO_2$ mixing ratios are determined against 4 working standard





ACPD
13, 22893–22930, 2013



gases, each a mixture of cleanup air and pure $CO_2$ filled in a 49 L aluminum cylinder. The $CO_2$ mixing ratios of the 4 working standard gases span about 50 ppm, and fully cover the range of atmospheric variations observed at HAT. These 4 working standard gases are replaced every 2–2.5 yr, and their mixing ratios are calibrated against the NIES 09 $CO_2$ standard scale (Machida et al., 2011) in our laboratory before and after every use at HAT. Before and after differences are less than 0.05 ppm.

To reduce water vapor in the sample air for $CH_4$ and CO measurements, we use a Nafion tube dryer and a cold trap (−40 °C). The dried air is then introduced into the $CH_4$ and CO analytical systems, separately. $CH_4$ and CO are semi-continuously measured by a gas chromatograph equipped with a flame ionization detector (GC/FID) and a gas chromatograph/mercury oxide (GC / HgO) analyzer (RGA3, Trace Analytical Co. Ltd., USA), respectively. The analytical precisions are about 2 nmol $mol^{-1}$ (ppb) for both $CH_4$ and CO measurements. The GC analysis interval for $CH_4$ and CO is 10 min, except during January 1996–November 1997, when the interval was 15 min for $CH_4$. Thus the $CH_4$ data before November 1997 are not used in this study because of the lower analysis frequency. Both the $CH_4$ and CO mixing ratios are determined against the working standard gases, each made up of a mixture of cleanup air and pure $CH_4$ or CO gases filled in a 49 L aluminum cylinder. These $CH_4$ and CO working standards are traceable to the NIES 94 $CH_4$ standard scale (Terao et al., 2011) and the NIES 09 CO standard scale (Katsumata et al., 2011), respectively.

For $CH_4$ measurements, we use 3 working standard gases with mixing ratios of about 1700, 1850, and 2000 ppb. Each set of 3 working standard gases are replaced every 5 yr at HAT. After December 2009, we have changed the volume of the working gas cylinder to 9.4 L, and have replaced the working standard gases every year. We have yet to observe any significant drift in these $CH_4$ working standard gases during use at HAT.

For CO measurements, we use 3 working standard gases with mixing ratios of about 80 ppb, 200 ppb and 400 ppb for the period 1999 to 2004. After September 2004, we have added a 4th CO standard gas with a mixing ratio of about 800 ppb. The procedural





ACPD
13, 22893–22930, 2013



protocol for the CO working gas is similar to that of the $CH_4$ working gas, and after December 2009, we have been using 9.4 L aluminum cylinders, instead of the 49 L cylinders, and are replacing them every year. Unfortunately, the working standards in all the 49 L aluminum cylinders, except one, showed significant drifts, ranging from 1 ppb $yr^{-1}$ to 16 ppb $yr^{-1}$. The drifts in the CO working reference gases during use at HAT have been determined in our laboratory by linear or quadratic interpolation based on the temporal changes in the CO mixing ratios before and after use at HAT. In order to validate the interpolated CO mixing ratios of the working standard gases, we compare the in-situ observation with flask sample measurements, which are collected primarily for $O_2$ / $N_2$ measurements at HAT (Tohjima et al., 2008). The CO mixing ratios from flask samples are measured by using a GC / HgO analyzer at our laboratory. The average and the standard deviation of the differences between the flask data and the corresponding in-situ hourly data are 0.3 ppb and 7.0 ppb, respectively, with 89 % of the differences lying within a range of ±10 ppb (Supplement S.1); the slope of the correlation plot is 1.008 ± 0.003 (Supplement S.2), giving confidence to the ability of our interpolation to accurately reflect the drift.

For this study, we use hourly averages of the atmospheric $CO_2$, $CH_4$, and CO mixing ratios observed at HAT for the correlation analysis. The study periods are from November 1997 to March 2010 for $CO_2$ and $CH_4$, and from November 1998 to March 2010 for CO (Fig. 2).

## 3 Methods of correlation analysis

Our focus is on the temporal change in the correlational relationship between $CO_2$, $CH_4$, and CO associated with synoptic-scale variations (SSVs) observed at HAT. Our calculation procedure begins with obtaining a best-fit smooth curve to each of the time series by using the methods of Thoning et al. (1989) with a cut-off frequency of 4.6 cycles $yr^{-1}$, and then subtracting it from the original time series. The residual time series are denoted as $\Delta CO_2$, $\Delta CH_4$ and $\Delta CO$. The hourly $\Delta CO_2$, $\Delta CH_4$, and $\Delta CO$





ACPD
13, 22893–22930, 2013



time series from 20 January to 11 February 2008 are shown in Fig. 3a as a typical example.

We then construct scatter plots of $\Delta CH_4$ vs. $\Delta CO_2$, $\Delta CO$ vs. $\Delta CO_2$, and $\Delta CO$ vs. $\Delta CH_4$ using the first 24 h of data. Reduced major axis (RMA) regression analysis is carried out on each scatter plot to obtain regression slopes ($\Delta CH_4 / \Delta CO_2$, $\Delta CO / \Delta CO_2$, and $\Delta CO / \Delta CH_4$ slopes) (Hirsh and Gilroy, 1984). We repeat the RMA analysis as we successively shift the 24 h time window by 1 h over the entire data record. If (i) the absolute value of the correlation coefficient is less than 0.8 ($|R|<0.8$), or (ii) the number of data is less than 5, or (iii) the standard deviation of $CO_2$ is less than 0.1 ppm ($1\sigma_{CO_2}<0.1$), then we deem the regression slope to be statistically insignificant and do not include it in the calculation of monthly averages of the correlation slopes. The RMA analysis is a relatively robust method of calculating the slope of two variables which show some causative relationship.

Figure 4 shows the average seasonal variation of the regression slopes. In the figure, each closed circle denotes the monthly average for the whole observation period, each error bar represents the standard deviation, and each black bar shows the number of regression slopes used to calculate the monthly average. The negative values of the average $\Delta CH_4 / \Delta CO_2$ and $\Delta CO / \Delta CO_2$ slopes in the summer are due to contribution from the enhanced terrestrial $CO_2$ uptake. We also note that the seasonal variation in the average $\Delta CO / \Delta CH_4$ slope may be attributable mainly to the large $CH_4$ flux seasonality with a maximum in the summer. However, it is possible that the seasonal CO flux from East Asia with higher flux in the winter than in the summer (Streets et al., 2003; Zhang et al., 2009) could partially contribute to the seasonality in the average $\Delta CO / \Delta CH_4$ slope.

The number of regression slopes with high correlation coefficients ($|R|>0.8$) decreases during the summer due to the predominant influence of maritime air masses from the Pacific at HAT (see Sect. 4.1). During the winter, fluxes from East Asia contribute to the short-term variations observed at HAT. But the monthly average slopes, especially $\Delta CH_4 / \Delta CO_2$, are relatively constant from late autumn to early spring (from





ACPD
13, 22893–22930, 2013



November to March), when the biotic activity is relatively dormant. These results seem to suggest that the emissions from East Asia during the 5-month winter period are relatively constant in time.

We now proceed to examine in detail the inter-annual variations in the correlation slopes observed at HAT during the 5-month winter period from November to March. Note that 2006/2007 winter, for example, indicates the period from November 2006 to March 2007.

## 4 Model simulation of correlation slopes

### 4.1 Concentration footprint for the measurements at HAT

In order to investigate the relationship between regional emissions and the correlation slopes observed at HAT, we employ FLEXPART ver. 8.0 (Stohl et al., 1998), a Lagrangian particle dispersion model. The model has been used to simulate the SSVs at HAT for $CO_2$ (Koyama et al., 2011), and for $CO_2$ and $O_2$ (Minejima et al., 2011). We compute concentration footprints that indicate the degree of sensitivity of each measurement to the surface fluxes upwind of the measurement site (HAT). To drive FLEXPART, we use six-hourly meteorology data with a spatial resolution of 1.25° × 1.25° from the JMA Climate Data Assimilation System (JCDAS) provided by the Japan Meteorological Agency (JMA). In each model run, 10 000 particles are released from 36.5 m above the ground level at HAT and transported back 8 days, giving enough time for particles to spread over East Asia. Footprints are prepared on a 0.5° × 0.5° grid for 1, 2, 3, . . . , 8 days back in time with a time resolution of 3 h from January 2006 to December 2010. Details of the model and simulation condition are described in Ganshin et al. (2012, 2013).

The average footprint for HAT during the 5-month winter period is shown in Fig. 5. The distribution of the footprint clearly shows that the emissions from East Asia have significant influence on the observation at HAT. The average correlation slopes from the





ACPD
13, 22893–22930, 2013



model are determined mostly by the emissions from the area with footprint larger than $1 \times 10^{-4}$ ppm (gC $m^{-2}$ $day^{-1})^{-1}$. Therefore, the area confined by the $1 \times 10^{-4}$ ppm (gC $m^{-2}$ $day^{-1})^{-1}$ contour line, is referred to hereafter as an effective footprint area (EFA) for the measurements at HAT. EFA includes North China, East China, Korea, Western Japan, and Taiwan.

### 4.2 Flux maps used in the model simulations

As part of the simulation procedure, we use fossil $CO_2$ emissions (fossil fuel burning and cement production) from the EDGAR ver. 4.2 $CO_2$ annual flux data (excluding short-cycle organic carbon from biomass burning) with a grid of 0.1° × 0.1° for the period 1997 to 2008. For our study, the spatial resolution of these annual fluxes is decreased to 0.5° × 0.5°. The emissions from China, Japan, Korea, Taiwan and the residual regions are then scaled to the national emission inventories from CDIAC (Carbon Dioxide Information Analysis Center, Boden et al., 2011) for the corresponding years. The fossil $CO_2$ flux maps for 2009 and 2010 are extrapolated from the 2008 EDGAR v4.2 emission map.

In addition to the fossil $CO_2$ fluxes, climatological monthly fluxes of the terrestrial biosphere from the optimized CASA (Carnegie-Ames-Stanford Approach) ecosystem model (Nakatsuka and Maksyutov, 2009) and of the oceanic air-sea exchange from Takahashi et al. (2009) are used. These data have a spatial resolution of 1° × 1°, and are applied year after year (no interannual variation) for simulating the atmopsheric $CO_2$ SSVs at HAT.

For $CH_4$, we use the monthly $CH_4$ emission maps gridded at 1° × 1° for 2007 taken from the emission scenario (E2 scenario) developed in Patra et al. (2009). For CO, we use the EDGAR v4.2 CO annual flux maps gridded at 0.1° × 0.1° for 2007. The spatial resolution of the CO flux map is decreased to a resolution of 0.5° × 0.5°.





ACPD
13, 22893–22930, 2013



### 4.3 Simulation of SSVs of $CO_2$, $CH_4$, and CO and their correlation analysis

In this study, we have been able to compute concentration footprints from January 2006 to December 2010 using FLEXPART. We then multiply these concentration footprints with the above mentioned fluxes to produce simulated time series of SSVs corresponding to individual fluxes. Chemical destruction of $CH_4$ and CO by hydroxyl radical (OH) during transport from the source regions to the receptor (HAT) are estimated by using OH concentration values at various latitudinal locations of the back trajectory in the boundary layer. The OH concentration data are obtained from the monthly climatological distributions of zonal mean OH (Spivakovsky et al., 2000). The reaction rate constants for $CH_4$ and CO with OH are obtained from the Jet Propulsion Laboratory database (Sander et al., 2006). Although the chemical reaction with OH does not significantly influence the simulated $CH_4$ concentration during its short transport time, it does reduce CO SSVs by about 5 % in the winter.

The simulated $CO_2$, $CH_4$, and CO variations for the same period as shown Fig. 3a are depicted in Fig. 3b. As can be seen in Fig. 3a and b, the model results are generally able to capture the observed pollution events with elevated mixing ratios. However, many of the details in the observed variations of the mixing ratios are not well reproduced, and the simulated amplitudes are generally underestimated, consistent with the results of previous studies (Koyama et al., 2011; Minejima et al., 2011). These discrepancies between the simulation and observation can be attributed to errors in the transport and/or fluxes used in the model simulation. Therefore, in this study, we have attempted to reduce the impact of transport errors by using correlation slopes to estimate regional emissions. It has been found that these correlation slopes are not strongly influenced by atmospheric transport under the assumption that the $CO_2$, $CH_4$ and CO fluxes have similar spatial distributions in East Asia (cf. Tohjima et al., 2010).

In order to evaluate the relationship between the East Asian emissions and the correlation slopes during the winter period, we calculate average correlation slopes from the simulated 5 yr SSVs for various sets of the above mentioned emissions. The average





ACPD
13, 22893–22930, 2013



correlation slopes are calculated as follows: time series of SSVs of $CO_2$ are obtained as a summed contribution from the fossil, oceanic, and land biotic $CO_2$ fluxes. From the simulated $CH_4$, CO, and combined $CO_2$ time series, we obtain correlation slopes of $\Delta CH_4 / \Delta CO_2$ and $\Delta CO / \Delta CO_2$, in the same way as the observed correlation slopes are calculated (see Sect. 3). We evaluate the winter average of the correlations slopes for the fossil emissions during 1998 to 2010 by using the corresponding time series of SSVs of the fossil $CO_2$. In this calculation, any influence of the year-to-year variation in the meteorological transport on the average correlation slopes appears as variability in the correlation slopes from the 5 yr simulated SSVs.

## 5 Results and discussion

### 5.1 Observed correlation slopes

Figure 6 shows the histograms of the correlation slopes derived from the observations made during the winter periods of 1998/1999 and 2009/2010 for $\Delta CH_4 / \Delta CO_2$, of 2001/2002 and 2009/2010 for $\Delta CO / \Delta CO_2$, and of 2003/2004 and 2009/2010 for $\Delta CO / \Delta CH_4$. These years are selected to highlight the extent of change in the distribution of the individual correlation slopes that has taken place over a decadal time scale. The correlation slopes of $\Delta CH_4 / \Delta CO_2$, $\Delta CO / \Delta CO_2$ and $\Delta CO / \Delta CH_4$ for the 2009/2010 winter have narrower distributions and lower average values than those of the earlier years. These changes are attributable to changes in the relative strengths of the emissions from EFA.

Temporal changes in the winter averages of the correlation slopes are depicted in Fig. 7. Tohjima et al. (2010) examined the inter-annual changes in the synoptic scale variations of $CO_2$ and $CH_4$ at HAT during a 6-month period (November to April) of each year from 1996 to 2007, and found that the $CO_2$ variability gradually increased relative to that of $CH_4$. They attributed the gradual increase to the recent rapid increase in the fossil fuel-derived $CO_2$ emissions from China (Gregg et al., 2008). Thus, the increase in





ACPD
13, 22893–22930, 2013



the $CO_2$ variability has caused the average $\Delta CH_4 / \Delta CO_2$ and $\Delta CO / \Delta CO_2$ correlation slopes shown in Fig. 7 to decrease gradually with time. The observed $\Delta CH_4 / \Delta CO_2$ and $\Delta CO / \Delta CO_2$ slopes decrease from about 12 ppb ppm$^{-1}$ to less than 10 ppb ppm$^{-1}$ and from about 45 ppb ppm$^{-1}$ to 30 ppb ppm$^{-1}$ during 1998–2010, respectively. But the rate of decrease is not the same for both. The $\Delta CH_4 / \Delta CO_2$ slope shows a relatively fast decrease during 1998–2005 and then levels off during 2005–2010, while the $\Delta CO / \Delta CO_2$ slope is relatively flat during 1999–2004 but then decreases quickly during 2004–2010. Unlike these trends, the average $\Delta CO / \Delta CH_4$ slope shows gradual increase during 1999–2004 and decrease during 2005–2010.

### 5.2 Simulated correlation slopes

As described in Sect. 4, we obtain correlation slopes from the simulated $CO_2$, $CH_4$, and CO SSVs, using a variety of fossil $CO_2$ emissions. In Fig. 7a and b, we also depict the winter averages of the simulated $\Delta CH_4 / \Delta CO_2$ and $\Delta CO / \Delta CO_2$ slopes. Both of the simulated slopes show similar decreasing trends. The temporal change in the simulated $\Delta CH_4 / \Delta CO_2$ slopes agrees well with the observed change, especially for the period 1998–2005. However, the leveling off of the observed trend during the period 2005–2010 is not simulated well.

The simulated $\Delta CO / \Delta CO_2$ slopes underestimate the observed slopes by about 30 % (Fig. 7b), suggesting that the $CO / CO_2$ emission ratio within EFA in the model is lower than the actual ratio. However, the overall decreasing trend pattern of the simulated $\Delta CO / \Delta CO_2$ slopes agrees generally with the observation. But the observed decreasing rate in the second period (2005–2010) seems to be larger than the simulated decreasing rate. The simulated $\Delta CO / \Delta CH_4$ slope based on the fixed emissions is also about half of the observed slopes (Fig. 7c).

The winter averages of the $CH_4 / CO_2$, $CO / CO_2$, and $CO/CH_4$ ratios of the EFA emissions used in the simulations are also plotted in Fig. 7. There are general agreements between the emission ratios and the simulated correlation slopes for the $CH_4 / CO_2$ ra-





ACPD
13, 22893–22930, 2013



tio, but the $CO/CO_2$ and $CO/CH_4$ emission ratios are about 20 % and 25 % lower than the simulated $\Delta CO/\Delta CO_2$ and $\Delta CO/\Delta CH_4$ correlation slopes, respectively. These higher simulated correlation slopes, despite the CO removal reaction with the OH radical in the model, can be explained by the more localized and heterogeneous distribution of CO emissions within EFA than $CH_4$ and $CO_2$.

### 5.3 Estimation of $CH_4$ and CO emissions from EFA

We estimate the year-to-year change in the emissions of $CH_4$ and CO from EFA so that the simulated $\Delta CH_4/\Delta CO_2$ and $\Delta CO/\Delta CO_2$ correlation slopes match the observations. We do this by adjusting single multiplying factors for the $CH_4$ and CO emissions. In this estimation, we assume that the flux maps of fossil $CO_2$ based on the EDGAR v4.2 flux map and the CDIAC database are correct. Additionally, we also assume, for ease of interpretation, no interannual variations in the terrestrial biospheric and oceanic $CO_2$ fluxes and in the meteorological fields.

The optimized winter $CH_4$ and CO emissions are simply extended to annual emissions. We can do this because the $CH_4$ emissions from biotic sources like rice fields have large seasonality, with highest emissions occurring in the summer. In China, $CH_4$ emissions from rice fields occur from April to October, and more than 70 % of the total emission happens between June and August, with about 90 % of it occurring in Southern China (between 23° N and 33° N) (Yan et al., 2003). Therefore, a large contribution to the observed $CH_4$ SSV at HAT during the winter comes from the non-seasonal $CH_4$ emissions from the anthropogenic sources, and not from biotic sources like the rice fields.

Inter-annual variations in the annual $CH_4$ and CO emissions are estimated using two scenarios: (1) S1 – changing the emissions from EFA and (2) S2 – changing only the emissions from China within EFA. The estimated emissions are depicted in Fig. 8, where the results from S1 and S2 are denoted by the closed squares and open circles, respectively. The error bars in the figure represent estimated uncertainties, which consist of uncertainties associated with the observed and simulated average correlation





ACPD
13, 22893–22930, 2013



slopes and the uncertainty (15 %) of the fossil fuel-derived $CO_2$ emissions from China (Gregg et al., 2008). In Fig. 8, we also plot the Chinese part of the EFA emissions in S1 as open squares. The $CH_4$ emissions from China estimated in S1 and S2, shown as open circles and open squares in Fig. 8a, agree to within ±3 % of each other. Similar results can be seen in the CO emissions from China (Fig. 8b) although the Chinese CO emissions in S2 are, on average, systematically higher by about 4 % than those in S1. These results seem to suggest that the emissions from EFA outside China contribute little to the observed changes in the average correlation slopes at HAT.

The estimated annual $CH_4$ emissions are relatively stable during 1998–2005 but increase during 2005–2010; for CO, it increases and decreases during 1999–2005 and 2005–2010, respectively. The annual $CH_4$ emission from China within EFA is about 21 $TgCH_4\,yr^{-1}$ during 1998–2005 and increases to about 27 $TgCH_4\,yr^{-1}$ in 2009/2010, but for CO it is about 100 $TgCO\,yr^{-1}$ in 1998/1999, increases to about 140 $TgCO\,yr^{-1}$ in 2004/2005, and then slightly decreases to about 120 $TgCO\,yr^{-1}$ in 2009/2010. The simulated $\Delta CO/\Delta CH_4$ slopes based on these optimized $CH_4$ and CO emissions from China within EFA (S2), plotted in Fig. 7 as open orange squares, show considerable agreement with the observations.

### 5.4 Comparison of the estimated emissions with other studies

The estimated $CH_4$ and CO emissions from China in the previous section are compared with the annual emissions from China estimated by other studies. Since we have optimized those Chinese emissions from EFA only (S2), we have added the emissions from China outside EFA (hereinafter referred to as the extended Chinese area (ECA)) to obtain an estimated national emission for the winter period. These additional emissions from ECA are computed from the $CH_4$ and CO flux maps prepared in Sect. 4.2. We thus obtain additional emissions of 18 $TgCH_4\,yr^{-1}$ and 31.6 $TgCO\,yr^{-1}$, which we assume to be constant over the study period. Our estimated $CH_4$ and CO emissions from China are summarized in Table 1 and plotted in Figs. 9 and 10, respectively. We





ACPD
13, 22893–22930, 2013



find that the estimated $CH_4$ and CO emissions from ECA contribute less than 47 % and 23 % to the total China emissions, respectively.

### 5.4.1 $CH_4$

Estimates of the $CH_4$ emission from Chinese anthropogenic sources without the rice fields taken from the inventory databases EDGAR ver. 4.2 and REAS ver. 1.11 (Regional Emission inventory in ASia, Ohara et al., 2007, http://www.jamstec.go.jp/frcgc/research/p3/emission.htm) are plotted for comparison with our results in Fig. 9. The REAS estimates are lower than our estimates. The EDGAR emission estimates show good agreement with our estimates for the period 1998 to 2002. However, after 2002 the EDAGAR data show a much faster increase of $3.1 \pm 0.1$ $TgCH_4\,yr^{-2}$ (2002–2008), which is about 3 times larger than our estimates of $1.1 \pm 0.2$ $TgCH_4\,yr^{-2}$ (2002–2010). According to the EDGAR ver. 4.2 database, about 70 % of the increase in the Chinese emission is attributed to the emissions related to fossil fuel production after 2002, and occurs mostly within EFA. Therefore, we suspect that the EDGAR ver. 4.2 inventory is overestimating the recent increase in the $CH_4$ emissions related to the fossil fuel production.

### 5.4.2 CO

The reported estimates of CO emission from China based on bottom-up and top-down approaches are plotted in Fig. 10, together with our estimates. The bottom-up estimates from REAS v1.11 and EDGAR v4.2 and other studies (Streets et al., 2003, 2006; Zhang et al., 2009) are plotted as circles in the figure. The top-down approach is divided into inverse modeling (Palmer et al., 2003; Wang et al., 2004; Heald et al., 2004; Yumimoto and Uno, 2006, 2012; Tanimoto et al., 2008; Kopacz et al., 2009) and forward modeling (Heald et al., 2003; Allen et al., 2004), which are plotted as squares and diamonds in the figure, respectively. These top-down emissions were estimated by using CO observations from aircrafts, ground-based stations, satellites, or any combi-





ACPD
13, 22893–22930, 2013



nation thereof. In general, our estimated emissions agree with these reported bottom-up and top-down estimations except those taken from the EDGAR ver. 4.2 database that shows about 40 % lower estimates than the other estimates including ours.

Our winter emission estimates would of course be biased if the CO emission has a noticeable seasonality. For example, inversely calculated regional emissions using satellite data have suggested that the areas where biomass burning dominates the CO emission have a large seasonal variation (Kopacz et al., 2010; Gonzi et al., 2011). However, the contribution of the biomass burning to the CO emission is relatively small for China, especially for EFA. Streets et al. (2003) showed also that the temperature dependence of the residential energy consumption could cause seasonality in the CO emissions from China. Using monthly data for power generation and industry, as well as residential energy consumption, Zhang et al. (2009) developed a dataset of monthly CO emissions from China, which shows a significant seasonality, with 17 % larger average monthly emission for our 5-month winter than for an entire year. If in fact there is a strong seasonal variation in the CO emission, then our winter estimate needs to be reduced by 17 %, which is still not large enough to explain the difference between our estimate and the EDGAR v4.2 estimate. Thus we conclude that EDGAR v4.2 overestimates the CO emission for China.

The TRACE-P (Transport and Chemical Evolution over the Pacific) campaign that was intensively conducted over the western Pacific in the spring of 2001, reported several CO emission estimates from China; these values are shown in Fig. 10. Those estimates range from 142 to 181 $TgCO\,yr^{-1}$, with lower values corresponding closely to the bottom-up estimates of REAS v1.1 and our estimates. The year-to-year variation in our emission estimates agree with the reported variation in the emission estimates during the period 1999–2010. The CO emission increase during 1999–2005 is easily understandable because fossil fuel consumption in China has steadily increased after 2000. The question is whether the CO emission from China has truly stopped increasing after 2005 in spite of the continued increase in the estimated fossil fuel consumption.





ACPD
13, 22893–22930, 2013



From the atmospheric $CO_2$, CO and $^{14}CO_2$ measurements at Tae-Ahn Peninsula in Korea (TAP) during 2004–2010, Turnbull et al. (2011) found that the emission ratio of CO to fossil fuel-derived $CO_2$ from China showed a gradual decrease during 2004–2006 and then plateaued from 2007 till 2009. For the usual 3-month winter season (December–February), Wang et al. (2010) showed that an average of the $CO/CO_2$ slopes observed at the Miyun site (located about 100 km northeast of the Beijing), also showed a decreasing trend from the 2004/2005 winter to the 2008/2009 winter, with the latter value being slightly larger than that for the 2007/2008 winter (Wang et al., 2010). They attributed these decreasing trends in the $CO/CO_2$ ratio to recent improvements in the fossil fuel combustion efficiency in China, corresponding in time to the implementation of air pollution reduction measures to improve the air quality in Beijing prior to the 2008 Summer Olympics and Paralympics Games.

Although the $CO/CO_2$ ratio values obtained by Wang et al. (2010) and Turnbull et al. (2011) showed a slight increase after 2008, the $\Delta CO/\Delta CO_2$ slopes at HAT in 2009–2010 show a substantial decrease compared to those of the preceding years. Top-down estimates based on the satellite data from Yumimoto and Uno (2012), although showing a slight increase during 2005–2007, also show a distinct decrease from 2007 to 2008 (shown as open blue squares with line in Fig. 10) and maintain the lower values during 2008–2010. This continued decrease seems to suggest that the overall combustion efficiency in China might still continue to improve even after the Olympics. However, as we noted above, the observed temporal changes in the $CO/CO_2$ slopes at HAT are mainly reflective of the year-to-year variation in the terrestrial $CO_2$ emission strength and atmospheric transport. For example, relative increases in the air mass transport from Korea and Japan, which have lower $CO/CO_2$ emission ratios than China, could reduce the $\Delta CO/\Delta CO_2$ slopes at HAT. Such issues will be examined in our future work.





ACPD
13, 22893–22930, 2013



## 6 Conclusions

We have examined the year-to-year changes in the average correlation slopes of $\Delta CH_4 / \Delta CO_2$, $\Delta CO / \Delta CO_2$ and $\Delta CO / \Delta CH_4$ for a 5-month winter from November to March observed at HAT over the last 10 yr. Consistent with the recent rapid increase in the fossil fuel $CO_2$ emissions from China, the observed $\Delta CH_4 / \Delta CO_2$ and $\Delta CO / \Delta CO_2$ slopes have correspondingly decreased. However, there are differences in the decreasing trends between $\Delta CH_4 / \Delta CO_2$ and $\Delta CO / \Delta CO_2$ slopes; the $\Delta CH_4 / \Delta CO_2$ slope levels off after 2005 while the $\Delta CO / \Delta CO_2$ slope plateaus from 1999 to 2004. These observational results may reflect differences in the inter-annual variations that are occurring between the emissions of $CH_4$ and CO from their source regions. Such different emission trends are also supported by the temporal changes observed in the $\Delta CO / \Delta CH_4$ slope, with an increasing trend during 1999–2004 and a decreasing trend during 2005–2010.

We have estimated the geographical distribution of the sensitivity of the winter measurements at HAT to the emissions from East Asia by using a Lagrangian particle dispersion model (FLEXPART) driven by meteorological data from 2006 to 2010. The average sensitivity distribution (average footprint) shows that the emissions from North and East China mostly contribute to the observed short-term variations at HAT. We have also evaluated the relationship between the emissions from East Asia and the correlation slopes at HAT by using FLEXPART and a set of previously reported emission maps. From the relationship, we have been able to obtain estimates of the $CH_4$ and CO emissions from China so that the simulated average $\Delta CH_4 / \Delta CO_2$ and $\Delta CO / \Delta CO_2$ slopes would match the observed slopes. In this calculation, we have assumed that there are no year-to-year variations in the land biotic and oceanic $CO_2$ emissions and that the fossil fuel derived $CO_2$ emissions change in accordance with the CDIAC database. The estimated $CH_4$ emissions from China, corresponding to emissions from non-seasonal sources or anthropogenic sources without rice fields, show a relatively constant value of about $39 \pm 6$ $TgCH_4\,yr^{-1}$ during 1998–2002, gradually increasing at a





ACPD
13, 22893–22930, 2013



rate of 1.1 ± 0.2 $TgCH_4\,yr^{-2}$ during 2002–2010, and then reaching 46 ± 7 $TgCH_4\,yr^{-1}$ in 2009/2010. This increasing rate of the Chinese $CH_4$ emissions for the decadal period under study is much smaller than that taken from the EDGAR V.4.2 database. However, these estimated $CH_4$ emission increases are not negligible in the context of the global $CH_4$ budget, and might substantially contribute to the recent atmospheric $CH_4$ increase (Rigby et al., 2008; Dlugokencky et al., 2009; Terao et al., 2011).

We have estimated the annual CO emissions from China to be 134 ± 26 $TgCO\,yr^{-1}$ in 1998/1999, increasing to 182 ± 33 $TgCO\,yr^{-1}$ in 2004/2005, plateauing during 2005–2008, and then decreasing to less than 160 $TgCO\,yr^{-1}$ after 2008/2009. In spite of the recent continued increase in fossil fuel consumption in China, our results have shown that the recent stagnation or decrease in the CO emission from China points to the possibility of a continued improvement in the combustion efficiency in that country, air pollution reduction measures that were implemented prior to the 2008 Olympics. Our CO emission estimates agree well with previously reported CO emission estimates, except for the CDIAC database which shows a value smaller than our estimates by about 30 $TgCO\,yr^{-1}$.

**Supplementary material related to this article is available online at http://www.atmos-chem-phys-discuss.net/13/22893/2013/acpd-13-22893-2013-supplement.pdf.**

*Acknowledgements.* We gratefully acknowledge Nobukazu Oda and other members of the Global Environment Forum and the staff of Center for Global Environmental Research for their continued support in maintaining the in-situ measurements of $CO_2$, $CH_4$ and CO at HAT. We also thank Hisayo Sandanbata and Yoko Kajita for the preparation and measurement of flask samples collected at HAT. Thanks are also expressed to Itsushi Uno and Keiya Yumimoto for helpful discussions on the temporal change in the CO emissions from China.





ACPD
13, 22893–22930, 2013



## References


Allen, D., Pickering, K., and Fox-Rabinovitz, K.: Evaluation of pollutant outflow and CO sources during TRACE-P using model-calculated, aircraft-based, and Measurements of Pollution in the Troposphere (MOPITT)-derived CO concentrations, J. Geophys. Res., 109, D15S03, doi:10.1029/2003JD004250, 2004.

Boden, T. A., Marland, G., and Andres, R. J.: Global, regional, and national fossil-fuel $CO_2$ emissions. Carbon Dioxide Information Analysis Center, Oak Ridge National Laboratory, U.S. Department of Energy, Oak Ridge, Tenn., USA, doi:10.3334/CDIAC/00001_V2011, 2011.

Dlugokencky, E. J., Masarie, K. A., Lang, P. M., and Tans, P. P.: Continuing decline in the growth rate of the atmospheric methane burden, Nature, 393, 447–450, 1998.

Dlugokencky, E. J., Houweling, S., Bruhwiler, L., Masarie, K. A., Lang, P. M., Miller, J. B., and Tans, P. P.: Atmospheric methane levels off: Temporary pause or a new steady-state?, Geophys. Res. Lett., 30, 1992, doi:10.1029/2003GL018126, 2003.

Dlugokencky E. J., Bruhwiler, L, White, J. W. C., Emmons, L. K., Novelli, P. C., Montzka, S. A., Masarie, K. A., Lang, P. M., Crotwell, A. M., Miller, J. B., and Gatti, L. V.: Observational constraints on recent increases in the atmospheric $CH_4$ burden, Geophys. Res. Lett., 36, L18803, doi:10.1029/2009GL039780, 2009.

Etheridge, D. M., Steele, L. P., Francy, R. J., and Langenfelds, L.: Atmospheric methane between 100 A. D. and present: Evidence of anthropogenic emissions and climatic variability, J. Geophys. Res., 103, 15979–15993 1998.

Ganshin, A., Oda, T., Saito, M., Maksyutov, S., Valsala, V., Andres, R. J., Fisher, R. E., Lowry, D., Lukyanov, A., Matsueda, H., Nisbet, E. G., Rigby, M., Sawa, Y., Toumi, R., Tsuboi, K., Varlagin, A., and Zhuravlev, R.: A global coupled Eulerian-Lagrangian model and 1 × 1 km $CO_2$ surface flux dataset for high-resolution atmospheric $CO_2$ transport simulations, Geosci. Model Dev., 5, 231–243, doi:10.5194/gmd-5-231-2012, 2012.

Ganshin, A. V., Zhuravlev, R. V., Maksyutov, Sh. Sh., Lukyanov, A. N., and Mukai, H.: Simulation of contribution of continental anthropogenic sources to variations in the $CO_2$ concentration during winter period on Hateruma Island, Atmos. Ocean. Opt., 26, 35–40, 2013.

Gonzi, S., Feng, L., and Palmer, P. I.: Seasonal cycle of emissions of CO inferred from MOPITT profiles of CO: Sensitivity to pyroconvection and profile retrieval assumptions, Geophys. Res. Lett., 38, L08813, doi:10.1029/2011GL046789, 2011.






ACPD
13, 22893–22930, 2013



Gregg, J. S., Andres, R. J., and Marland, G.: China: Emissions pattern of the world leader in $CO_2$ emissions from fossil fuel consumption and cement production, Geophys. Res. Lett., 35, L08806, doi:10.1029/2007GL032887, 2008.

Heald, C. L., Jacob, D. J., Fiore, A. M., Emmons, L. K., Gille, J. C., Deeter, M. N., Warner, J., Edwards, D. P., Crawford, J. H., Hamlin, A. J., Sachse, G. W., Browell, E. V., Avery, M. A., Vay, S. A., Westberg, D. J., Blake, D. R., Singh, H. B., Sandholm, S. T., Talbot, R. W., and Fuelberg, H. E.: Asian outflow and tran-integrated satellite, aircraft, and model perspective, J. Geophys. Res., 108, 4804, doi:10.1029/2003JD003507, 2003.

Heald, C. L., Jacob, D. J., Jones, D. B. A., Palmer, P. I., Logan, J. A., Streets, D. G., Sachse, G. W., Gille, J. C., Hoffman, R. N., and Nehrkorn, T.: Comparative inverse analysis of satellite (MOPITT) and aircraft (TRACE-P) observations to estimate Asian sources of carbon monoxide, J. Geophys. Res., 109, D23306, doi:10.1029/2004JD005185, 2004.

Hirsch, R. M. and Gilroy, E. J.: Methods of fitting a straight line to data: Examples in water resources, Water Resour. Bull., 20, 705–711, 1984.

Katsumata, K., Machida, T., Tanimoto, H., Nara, H., and Mukai, H.: Re-evaluation of NIES CO scale using high concentration gravimetric CO standard gases, Paper presented at: Report of the 15th WMO Meeting of Experts on Carbon Dioxide Concentration and Related Tracer Measurement Techniques; September2009; Jena, Germany, WMO/GAW Rep. 194, edited by: Brand, W., 295–298, WMO, Geneva, Switzerland, 2011.

Kopacz, M., Jacob, D. J., Henze, D. K., Heald, C. L., Streets, D. G., and Zhang, Q.: Comparison of adjoint and analytical Bayesian inversion methods for constraining Asian sources of carbon monoxide using satellite (MOPITT) measurements of CO columns, J. Geophys. Res., 114, D04305, doi:10.1029/2007JD009264, 2009.

Kopacz, M., Jacob, D. J., Fisher, J. A., Logan, J. A., Zhang, L., Megretskaia, I. A., Yantosca, R. M., Singh, K., Henze, D. K., Burrows, J. P., Buchwitz, M., Khlystova, I., McMillan, W. W., Gille, J. C., Edwards, D. P., Eldering, A., Thouret, V., and Nedelec, P.: Global estimates of CO sources with high resolution by adjoint inversion of multiple satellite datasets (MOPITT, AIRS, SCIAMACHY, TES), Atmos. Chem. Phys., 10, 855–876, doi:10.5194/acp-10-855-2010, 2010.

Koyama, Y., Maksyutov, S., Mukai, H., Thoning, K., and Tans, P.: Simulation of variability in atmospheric carbon dioxide using a global coupled Eulerian – Lagrangian transport model, Geosci. Model Dev., 4, 317–324, doi:10.5194/gmd-4-317-2011, 2011.





ACPD
13, 22893–22930, 2013



Levin, I., Kromer, B., Schmidt, M.,, and Sartorius, H.: A novel approach for independent budgeting of fossil fuel $CO_2$ over Europe by $^{14}CO_2$ observations, Geophys. Res. Lett., 30, 2194, doi:10.1029/2003GL018477, 2003.

Logan, J. A., Prather, M. J., Wofsy, S. C., and McElroy, M. B.: Tropospheric chemistry-A global perspective, J. Geophys. Res., 104, 26245–26277, 1981.

Machida, T., Tohjima, Y., Katsumata, K., and Mukai, H.: A new $CO_2$ calibration scale based on gravimetric one-step dilution cylinders in National Institute for Environmental Studies-NIES09 $CO_2$ scale. Paper presented at: Report of the 15th WMO Meeting of Experts on Carbon Dioxide Concentration and Related Tracer Measurement Techniques; September2009; Jena, Germany, WMO/GAW Rep. 194, edited by: Brand, W., 165–169, WMO, Geneva, Switzerland, 2011.

Minejima, C., Kubo, M., Tohjima, Y., Yamagishi, H., Koyama, Y., Maksyutov, S., Kita, K., and Mukai, H.: Analysis of $\Delta O_2/\Delta CO_2$ ratios for the pollution events observed at Hateruma Island, Japan, Atmos. Chem. Phys., 12, 2713–2723, doi:10.5194/acp-12-2713-2012, 2012.

Mukai, H., Katsumoto, M., Ide, R., Machida, T., Fujinuma, Y., Nojiri, Y., Inagaki, M., Oda, N., and Watai, T.: Characterization of atmospheric $CO_2$ observed at two-background air monitoring stations (Hateruma and Ochi-ishi) in Japan. Paper presented at: Sixth International Carbon Dioxide Conference; October 2001; Sendai, Japan, 2001.

Nakatsuka, Y. and Maksyutov, S.: Optimization of the seasonal cycles of simulated $CO_2$ flux by fitting simulated atmospheric $CO_2$ to observed vertical profiles, Biogeosciences, 6, 2733–2741, doi:10.5194/bg-6-2733-2009, 2009.

Nakazawa, T., Machida, T., Tanaka, M., Fujii, Y., Aoki, S., and Watanabe, O.: Differences of the atmospheric $CH_4$ concentration between the Arctic and Antarctic regions in pre-industrial/pre-agricultural era, Geophys. Res. Lett., 20, 943–946, 1993.

Ohara, T., Akimoto, H., Kurokawa, J., Horii, N., Yamaji, K., Yan, X., and Hayasaka, T.: An Asian emission inventory of anthropogenic emission sources for the period 1980–2020, Atmos. Chem. Phys., 7, 4419–4444, doi:10.5194/acp-7-4419-2007, 2007.

Palmer, P. I., Jacob, D. J., Jones, D. B. A., Heald, C. L., Yantosca, R. M., Logan, J. A., Sachse, G. W., and Streets, D. G.: Inverting for emissions of carbon monoxide from Asia using aircraft observations over the western Pacific, J. Geophys. Res., 108, 8828, doi:10.1029/2003JD003397, 2003.

Patra, P. K., Takigawa M., Ishijima, K., Choi, B.-C., Cunnold, D., Dlugokencky, E. J., Fraser, P., Gomez-Pelaez, A. J., Goo, T.-Y., Kim, J.-S., Krummel, P., Langenfelds, R., Meinhardt,





ACPD
13, 22893–22930, 2013



F., Mukai, H., O'Doherty, S., Prinn, R. G., Simmonds, P., Steele, P., Tohjima. Y., Tsuboi, K., Uhse, K., Weiss, R., Worthy, D., and Nakazawa, T.: Growth rate, seasonal, synoptic, diurnal variations and budget in lower atmospheric methane, J. Meteorol. Soc. Japan, 87, 635–663, doi:10.2151/jmsj.87.635, 2009.

Rigby, M., Prinn, R. G., Fraser, P. J., Simmonds, P. G., Langenfelds, R. L., Huang, J., Cunnold, D. M., Steele, L. P., Krummel, P. B., Weiss, R. F., O'Doherty, S., Salameh, P. K., Wang, H. J., Harth, C. M., Mühle, J., and Porter, L., W.: Renewed growth of atmospheric methane, Geophys. Res. Lett., 35, L22805, doi:10.1029/2008GL036037, 2008.

Sander, S. P., Friedl, R. R., Golden, D. M., Kuryolo, M. J., Moortgat, G. K., Keller-Rudek, H., Wine, P. H., Ravishankara, A. R., Kolb, C. E., Molina, M. J., Finlayson-Pitts, B. J., Huie, R. E., and Orkin, V. L.: Chemical kinetics and photochemical data for use in atmospheric studies, Jet Propul. Lab., Pasadena, CA, Rep. 06-2, 523 pp., 2006.

Schmidt, M., Graul, R., Sartorius, H., and Levin, I.: The Schauinsland $CO_2$ record: 30 years of continental observations and their implications for the variability of the European $CO_2$ budget, J. Geophys. Res., 108, 4619, doi:10.1029/2002JD003085, 2003.

Spivakovsky, C. M., Logan, J. A., Montzka, S. A., Balkanski, Y. J., Foreman-Fowler, M., Jones, B. A., Horowitz, L. W., Fusco, A. C., Brenninkmeijer, C. A. M., Prather, M. J., Wofsy, S. C., and McElroy, M. B.: Three dimensional climatological distribution of tropospheric OH: Update and evaluation, J. Geophys. Res., 105, 8931–8980, doi:10.1029/1999JD901006, 2000.

Steele, L. P., Dlugokencky, E. J., Lang, P. M., Tans, P. P., Martin, R. C., and Masarie, K. A.: Slowing down of the global accumulation of atmospheric methane during the 1980's, Nature, 358, 313–316, 1992.

Stohl, A., Hittenberger, M., and Wotawa, G.: Validation of the Lagrangian particle dispersion model FLEXPART against large-scale tracer experiment data, Atmos. Environ., 32, 4245–4264, 1998.

Streets, D. G., Bond, T. C., Carmichael, G. R., Fernandes, S. D., Fu, Q., He, D., Klimont, Z., Nelson, S. M., Tsai, N. Y., Wang, M. Q., Woo, J.-H., and Yarber, K. F.: An inventory of gaseous and primary aerosol emissions in Asia in the year 2000, J. Geophys. Res., 108, 8809, doi:10.1029/2002JD003093, 2003.

Streets, D. G., Zhang, Q., Wang, L., He, K., Hao, J., Wu, Y., Tang, Y., and Carmichael, G. R.: Revisiting China's CO emissions after the Transport and Chemical Evolution over the Pacific (TRACE-P) mission: Synthesis of inventories, atmospheric modeling , and observations, J. Geophys. Res., 111, D14306, doi:10.1029/2006JD007118, 2006.





ACPD
13, 22893–22930, 2013



Tanimoto, H., Sawa, Y., Yonemura, S., Yumimoto, K., Matsueda, H., Uno, I., Hayasaka, T., Mukai, H., Tohjima, Y., Tsuboi, K., and Zhang, L.: Diagnosing recent CO emissions and ozone evolution in East Asia using coordinated surface observations, adjoint inverse modeling, and MOPITT satellite data, Atmos. Chem. Phys., 8, 3867–3880, doi:10.5194/acp-8-3867-2008, 2008.

Tanimoto, H., Tohjima, Y., Mukai, H., Nara, H., and Hashimoto, S.: Anomalous geographical gap in carbon monoxide mixing ratios over Hokkaido (Japan) in summer 2004, Geochem., J., 43, e23–e29, 2009.

Takahashi, T., Sutherland, S. C., Wanninkhof, R., Sweeney, C., Feely, R. A., Chipman, D. W., Hales, B., Friederich, G., Chavez, F., Sabine, C., Watson, A., Bakker, D. C. E., Schuster, U., Metzl, N., Yoshikawa-Inoue, H., Ishii, M., Midorikawa, T., Nojiri, Y., Körtzinger, A., Steinhoff, T., Hoppema, M., Olafsson, J., Arnarson, T. S., Tilbrook, B., Johannessen, T., Olsen, A., Bellerby, R., Wong, C. S., Delille, B., Bates, N. R., and de Baar, H. J. W.: Climatological mean and decadal change in surface ocean $pCO_2$, and net sea-air $CO_2$ flux over the global oceans, Deep-Sea Res.II, 56, 554–577, doi:10.1016/j.dsr2.2008.12.009, 2009.

Terao, Y., Mukai, H., Nojiri, Y., Machida, T., Tohjima, Y., Saeki, T., and Maksyutov, S.: Interannual variability and trends in atmospheric methane over the western Pacific from 1994 to 2010, J. Geophys. Res., 116, D14303, doi:10.1029/2010JD015467, 2011.

Thompson, A. M.: The oxidizing capacity of the Earth's atmosphere-Probable past and future changes, Science, 256, 1157–1165, 1992.

Thoning, K., Tans, P. P., and Komhyr, W. D.: Atmospheric carbon dioxide at Mauna Loa Observatory 2. Analysis of the NOAA GMCC data, 1974–1985, J. Geophys. Res., 94, 8549–8565, 1989.

Tohjima, Y., Machida, T., Utiyama, M., Katsumoto, M., Fujinuma, Y., and Maksyutov, S.: Analysis and presentation of in situ atmospheric methane measurements from Cape Ochi-ishi and Hateruma Island, J. Geophys. Res., 107, ACH 8-1–ACH 8-11, doi:10.1029/2001JD001003, 2002.

Tohjima, Y., Mukai, H., Nojiri, Y., Yamagishi, H., and Machida, T.: Atmospheric $O_2/N_2$ measurements at two Japanese sites: Estimation of global oceanic and land biotic carbon sinks and analysis of the vaiations in atmospheric potential oxygen (APO), Tellus, 60B, 213–225, doi:10.1111/j.1600-0889.2007.00334.x, 2008.





ACPD
13, 22893–22930, 2013



Tohjima, Y., Mukai, H., Hashimoto, S., and Patra, P. K.: Increasing synoptic scale variability in atmospheric $CO_2$ at Hateruma Island associated with increasing East-Asian emissions, Atmos. Chem. Phys., 10, 453–462, doi:10.5194/acp-10-453-2010, 2010.

Turnbull, J. C., Tnas, P. P., Lehman, S. J., Baker, D., Conway, T. J., Chung, Y. S., Gregg, J., Miller, J. B., Southon, J. R, and Zhou, L.-X.: Atmospheric observations of carbon monoxide and fossil fuel $CO_2$ emissions from East Asia, J. Geophys. Res., 116, D24306, doi:10.1029/2011JD016691, 2011.

Wada, A, Matsueda, H., Murayama, S., Taguchi, S., Hirao, S., Yamazawa, H., Moriizumi, J., Tsuboi, K., Niwa, Y., and Sawa, Y.: Quantification of emission estimates of $CO_2$, $CH_4$ and CO for East Asia derived from atmospheric radon-222 measurements over the western North Pacific, Tellus B, 65, 18037, doi:10.3402/tellusb.v65i0.18037, 2013.

Wang, Y. X., McElroy, M. B., Wang, T., and Palmer, P. I.: Asian emissions of CO and $NO_x$: Constraints from aircraft and Chinese station data, J. Geophys. Res., 109, D24304, doi:10.1029/2004JD005250, 2004.

Wang, Y., Munger, J. W., Xu, S., McElroy, M. B., Hao, J., Nielsen, C. P., and Ma, H.: $CO_2$ and its correlation with CO at a rural site near Beijing: implications for combustion efficiency in China, Atmos. Chem. Phys., 10, 8881–8897, doi:10.5194/acp-10-8881-2010, 2010.

Worthy D. E. J., Chan E., Ishizawa M., Chan D., Poss C., Dlugokencky E. J., Maksyutov S., and Levin I.: Decreasing anthropogenic methane emissions in Europe and Siberia inferred from continuous carbon dioxide and methane observations at Alert, Canada, J Geophys Res., 114, D10301, doi:10.1029/2008JD011239, 2009.

Yan, X., Cai, Z., Ohara, T., and Akiomoto H.: Methane emission from rice fields in mainland China: Amount and seasonal and spatial distribution, J. Geohys, Res., 108, 4005, doi:10.1029/2002JD003182, 2003.

Yokouchi, Y., Taguchi, S., Saito, T., Tohjima, Y., Tanimoto, H., and Mukai, H.: High frequency measurements of HFCs at a remote site in east Asia and their implications for Chinese emissions, Geophys, Res. Lett., 33, L21814, doi:10.1029/2006GL026403, 2006.

Yumimoto, K. and Uno, I.: Adjoint inverse modeling of CO emissions over the East Asian region using four dimensional variational data assimilation, Atmos. Environ., 40, 6836–6845, 2006.

Yumimoto, K. and Uno, I.: Inverse estimate of long-term CO emission in China between 2005-2010 with Green's Function Method, J. Japan. Soc. Atmos. Environ., 47, 2012 (in Japanese with English abstract).





ACPD
13, 22893–22930, 2013



Zhang, Q., Streets, D. G., Carmichael, G. R., He, K. B., Huo, H., Kannari, A., Klimont, Z., Park, I. S., Reddy, S., Fu, J. S., Chen, D., Duan, L., Lei, Y., Wang, L. T., and Yao, Z. L.: Asian emissions in 2006 for the NASA INTEX-B mission, Atmos. Chem. Phys., 9, 5131–5153, doi:10.5194/acp-9-5131-2009, 2009.





ACPD
13, 22893–22930, 2013



**Table 1.** Summary of the estimated $CH_4$ and CO emissions from China[a].

| Year | Fossil fuel $CO_2$[b] | $CH_4$[c, d] | CO[d] |
|---|---|---|---|
| 1997/1998 | 0.93 | 38.4 ± 6.2 | |
| 1998/1999 | 0.91 | 40.5 ± 6.5 | 134 ± 26 |
| 1999/2000 | 0.92 | 37.3 ± 6.1 | 149 ± 27 |
| 2000/2001 | 0.94 | 39.4 ± 6.3 | 140 ± 29 |
| 2001/2002 | 0.98 | 39.1 ± 6.4 | 153 ± 29 |
| 2002/2003 | 1.12 | 37.3 ± 5.9 | 158 ± 28 |
| 2003/2004 | 1.34 | 40.7 ± 6.7 | 179 ± 34 |
| 2004/2005 | 1.51 | 39.4 ± 6.2 | 182 ± 33 |
| 2005/2006 | 1.66 | 44.0 ± 6.7 | 176 ± 31 |
| 2006/2007 | 1.80 | 43.3 ± 6.7 | 169 ± 29 |
| 2007/2008 | 1.88 | 44.7 ± 6.9 | 181 ± 32 |
| 2008/2009 | 1.98 | 46.5 ± 7.2 | 150 ± 26 |
| 2009/2010 | 2.14 | 45.8 ± 7.2 | 159 ± 28 |

[a] Values for $CO_2$ are given in PgC $yr^{-1}$, for $CH_4$ in $TgCH_4$ $yr^{-1}$, and for CO in TgCO $yr^{-1}$. [b] Fossil $CO_2$ emissions are taken from the CDIAC database. Each value is the average of the emissions for the consecutive two years described in the first column. The uncertainty is assumed to be 15 %, which is the lower limit of the estimation of Gregg et al. (2008). [c] Values represent the emissions from non-seasonal $CH_4$ sources (see text). [d] Uncertainties are calculated from the uncertainties of the fossil fuel-derived $CO_2$ emissions in China, the observed correlation slopes, and the simulated correlation slopes.





ACPD
13, 22893–22930, 2013



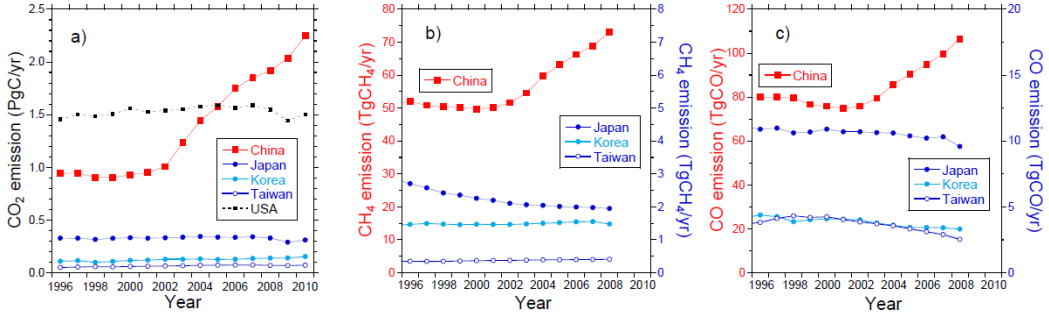


**Fig. 1.** Temporal changes in the estimated emissions of **(a)** fossil fuel-derived $CO_2$, **(b)** $CH_4$, and **(c)** CO from China, Japan, Korea, and Taiwan. The $CO_2$ emissions are taken from the CDIAC database. $CH_4$ and CO emissions are taken from EDGAR ver. 4.2. $CH_4$ and CO emissions from Japan, Korea and Taiwan are plotted against the right *y* axis. The fossil fuel-derived $CO_2$ emissions from USA are also plotted for comparison.





ACPD
13, 22893–22930, 2013



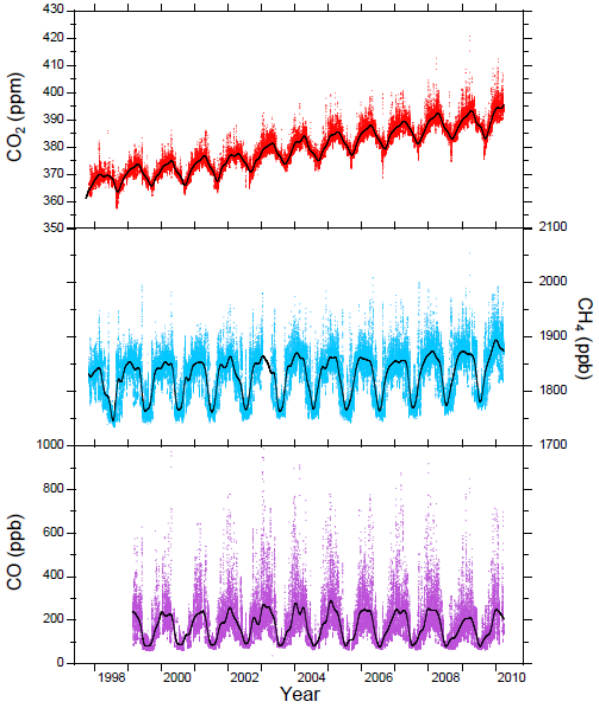


**Fig. 2.** Time series of atmospheric (top) $CO_2$, (middle) $CH_4$, and (bottom) CO mixing ratios observed at HAT. Each dot represents hourly average. Black lines represent the smooth curve fits to the data.





ACPD
13, 22893–22930, 2013



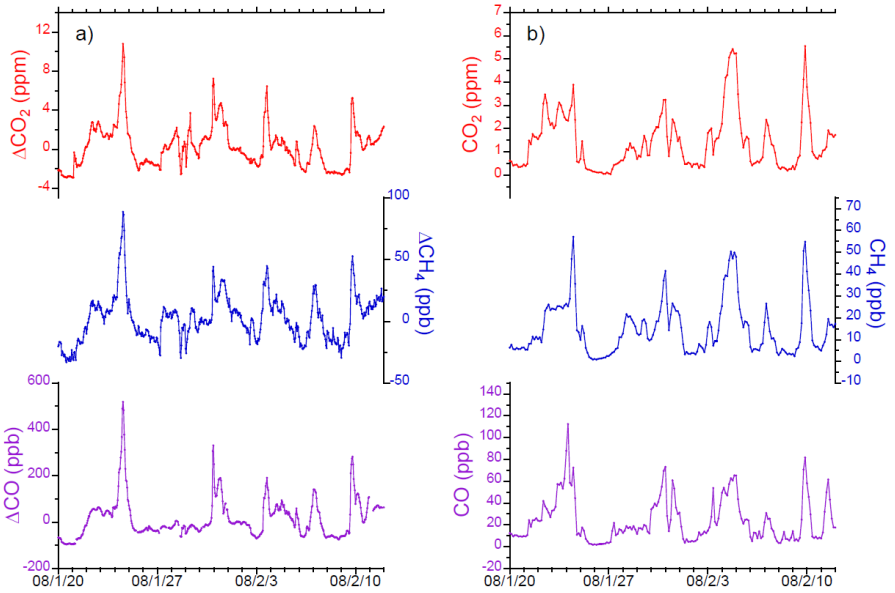


**Fig. 3.** Synoptic scale variations in hourly (top) $CO_2$, (middle) $CH_4$, and (bottom) CO based on **(a)** the observation and **(b)** the model simulation for the period from 20 January to 12 February 2008.





ACPD
13, 22893–22930, 2013



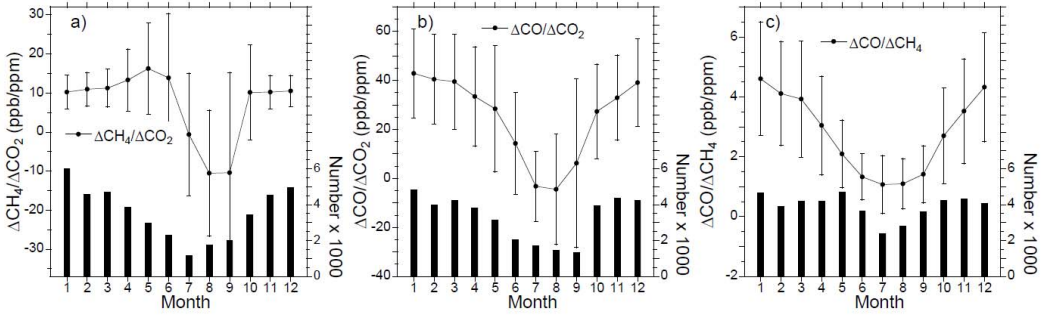


**Fig. 4.** Average seasonal variation of **(a)** $\Delta CH_4 / \Delta CO_2$, **(b)** $\Delta CO / \Delta CO_2$, and **(c)** $\Delta CO / \Delta CH_4$ slopes observed at HAT. The error bars represent the standard deviations from the monthly averages. The vertical bars represent the data number.





ACPD
13, 22893–22930, 2013



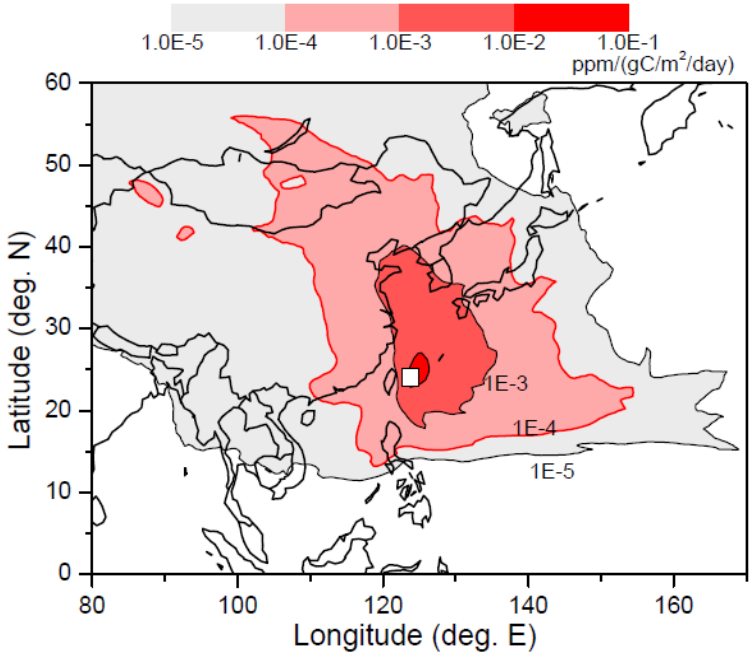


**Fig. 5.** Average footprint (ppm (gC $m^{-2}$ $day^{-1}$)$^{-1}$) for the measurements at HAT during the winter period (November to March). Meteorological data for 2006–2010 are used for the calculation. The location of HAT is indicated by the square. The area surrounded by the red thick contour lines of 1 × $10^{-4}$ ppm (gC $m^{-2}$ $day^{-1}$)$^{-1}$ is defined as an effective foot print area (EFA).





ACPD
13, 22893–22930, 2013



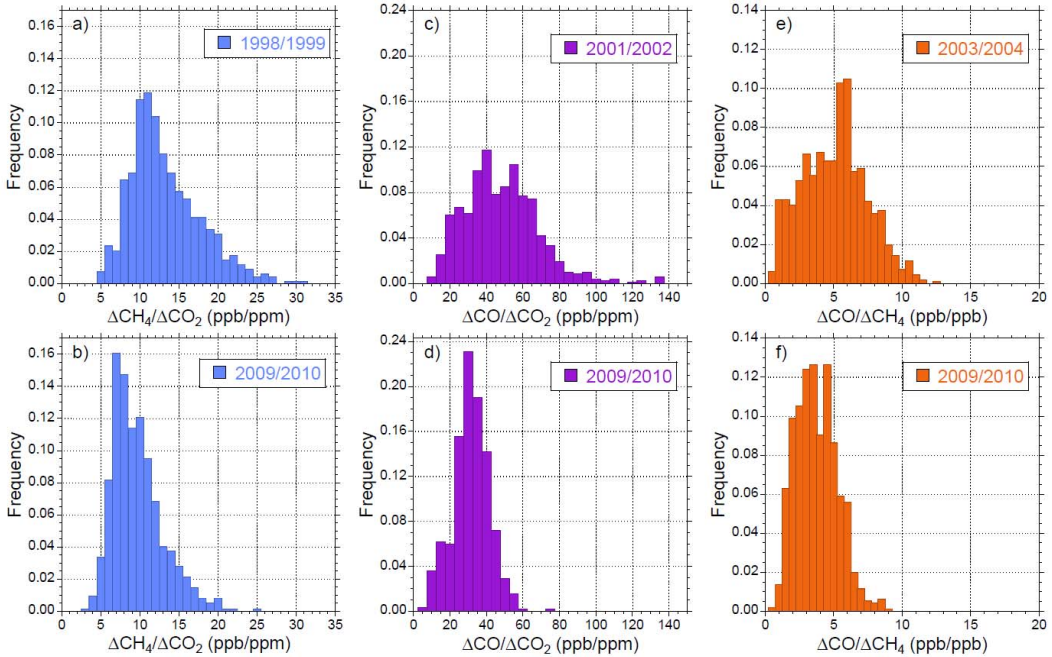


**Fig. 6.** Histograms of the correlation slops of **(a, b)** $\Delta CH_4 / \Delta CO_2$, **(c, d)** $\Delta CO / \Delta CO_2$, and **(e, f)** $\Delta CO / \Delta CH_4$ for the selected two periods. The correlation slopes all meet the selection criteria (see text).





ACPD
13, 22893–22930, 2013



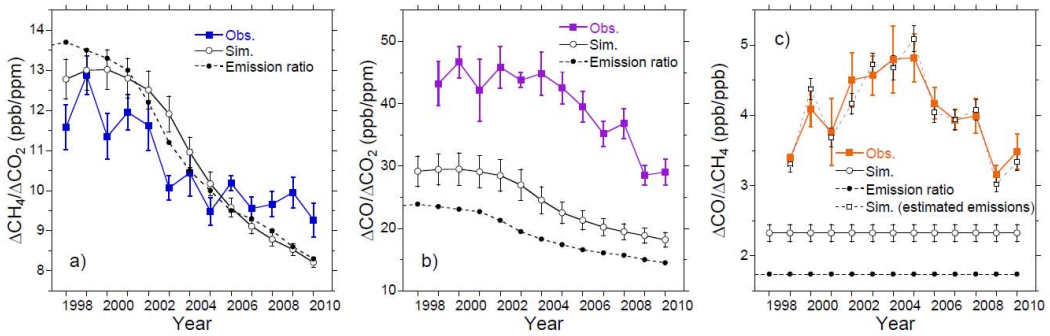


**Fig. 7.** Temporal changes in the winter average correlation slopes of **(a)** $\Delta CH_4 / \Delta CO_2$, **(b)** $\Delta CO / \Delta CO_2$, and **(c)** $\Delta CO / \Delta CH_4$. The closed squares represent the observation and the open circles represent the simulation. The error bars represent the standard errors. The ratios of the emissions within EFA are also depicted as closed circles.





ACPD
13, 22893–22930, 2013



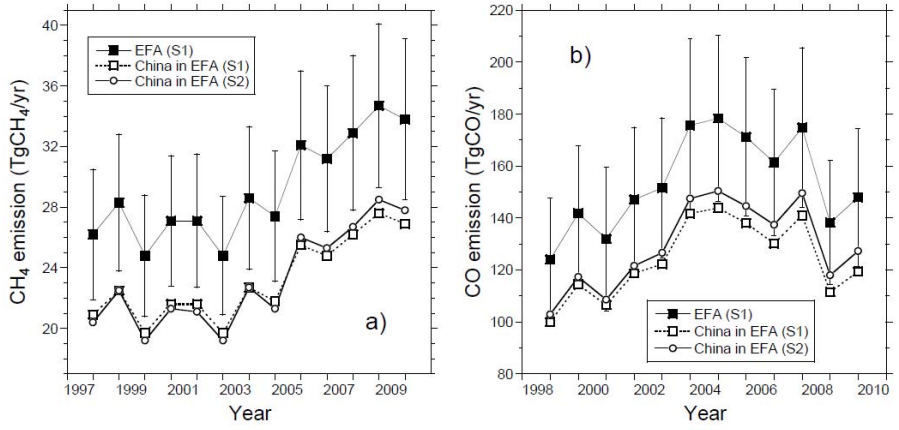


**Fig. 8.** Temporal changes in the estimated **(a)** $CH_4$ and **(b)** CO emissions from EFA. The emissions from EFA for S1 are depicted by closed squares with uncertainties. The emissions from China in EFA are depicted for S1 by open squares and for S2 by open circles (see text).





ACPD
13, 22893–22930, 2013



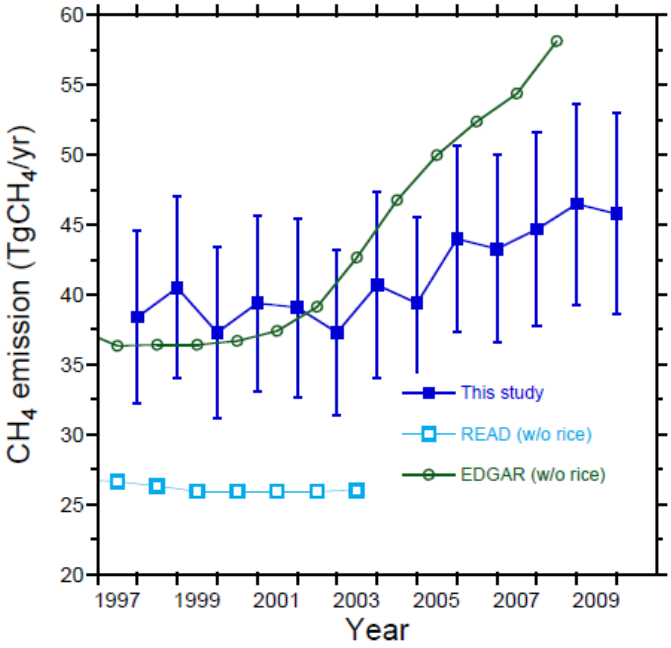


**Fig. 9.** Comparison of estimated non-seasonal $CH_4$ emissions from China. The values are expressed as annual emissions. Closed blue squares are the estimated emissions of this study. Open light blue squares and open green circles represent the $CH_4$ emissions from anthropogenic sources (excluding rice fields) in China based on the emission inventories from REAS ver 1.11. (Ohara et al., 2007) and EDGAR ver. 4.2 (http://edgar.jrc.ec.europa.eu/), respectively.





ACPD
13, 22893–22930, 2013



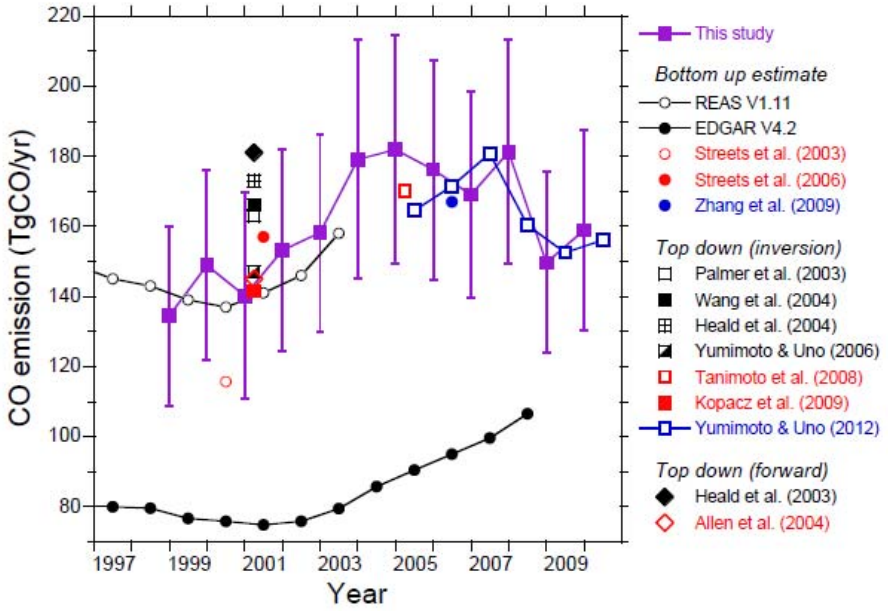


**Fig. 10.** Comparison of estimated CO emissions from China. The values are expressed as annual emissions. Closed blue squares are the estimated emissions of this study. Circles, squares, and diamonds represent the bottom up estimates, top down (inversion), and top down (forward) estimates, respectively.





ACPD
13, 22893–22930, 2013